Reorientation of the Retinylidene Chromophore in the K, L, and M Intermediates of Bacteriorhodopsin from Time-Resolved Linear Dichroism: Resolving Kinetically and Spectrally Overlapping Intermediates of Chromoproteins

Berthold Borucki, Harald Otto, and Maarten P. Heyn*

Biophysics Group, Physics Department, Freie Universität Berlin, Arnimallee 14, D-14195 Berlin, Germany

Received: February 24, 1999; In Final Form: May 19, 1999

We determined the change in orientation of the electronic transition dipole moment with respect to the membrane normal in the K, L, and M intermediates of bacteriorhodopsin using transient linear dichroism. Purple membranes were oriented in a 14 T magnetic field and immobilized in a gel. The oriented purple membranes were excited isotropically and the transient absorbance changes were detected with the sample between two parallel polarizers. The absorbance changes were measured as a function of wavelength, time, and angle between the orientation axis and polarizer direction. In this way, the transient changes in isotropic absorbance, linear dichroism, and linear birefringence were determined with high accuracy. The Kramers−Kronig transform of the transient linear dichroism was in excellent agreement with the transient linear birefringence and this served as a useful control on the reliability of the linear dichroism data. We developed a novel formalism to extract the anisotropies, spectra and time courses of the photocycle intermediates in a model−independent way from the combined analysis of the transient absorbance and linear dichroism data. Whereas an analysis based on transient absorbance data alone is underdetermined, we show that in combination with transient linear dichroism data a unique solution may be obtained for the early intermediates K, L, and M. The analysis makes use of the constraints that (1) the sum of the populations of the K, L, and M intermediates is constant in time and (2) the absorption for the M intermediate vanishes for $\lambda \geq 520$ nm. For wild-type bR at pH 7 (10 °C) we obtained in this way the following wavelength-independent anisotropies for the main absorption band: $r_{bR} = -0.145$, $r_K = -0.140$, $r_L = -0.132$, and $r_M = -0.139$. Similar experiments were carried out for the mutant D96A which allows more accurate experiments for the L and M intermediates under various conditions of temperature and pH (pH 7, 20 °C; pH 4.7, 20 °C; pH 4.7, 10 °C). In all cases there are very clear differences in the anisotropies and the sequence is always $r_{bR} < r_K < r_M < r_L$. The data analysis is validated by the fact that the spectra and time courses of the intermediates are in excellent agreement with previous work. Making the reasonable assumption that the order parameter characterizing the orientational distribution is the same for each intermediate, the anisotropy changes translate into small orientational changes for the transition dipole moment: $\Delta\theta_K = -0.8 \pm 0.2°$, $\Delta\theta_L = -1.7 \pm 0.2°$, $\Delta\theta_M = -1.1 \pm 0.3°$. The largest change occurs in the L intermediate. The angle with respect to the membrane normal is smaller in every intermediate than in the ground state. The simplest interpretation of the results is that after the isomerization of the $C_{13}-C_{14}$ double bond the C_5-N direction remains approximately the same with the C_5-C_{13} part of the polyene chain tilting out of the plane of the membrane.

1. Introduction

Structural changes of the chromophore play an important role in the function of photoactive proteins. In the photocycle of bacteriorhodopsin for example the isomerization of the retinal−chromophore is an essential step in the mechanism of proton transport.[1] Chromophore isomerization also plays a central role in the activation of the signal transduction proteins rhodopsin[2] and phytochrome.[3] The photoactive yellow protein provides another example of a large light−induced chromophore reorientation associated with isomerization.[4,5] These chromophore reorientations which are due to isomerization and subsequent protein relaxation are expected to lead to changes in the orientation of the electronic transition dipole moment in the various photointermediates. The dynamics of these orientational changes may be monitored by time-resolved absorption spectroscopy with linearly polarized light. Various approaches have been used. Photoselection with linearly polarized flash excitation of isotropic purple membrane samples[6−8] provides information about Ω_{0i}, the angle between the transition dipole moment in the initial state 0 and the intermediate state *i*. The use of near-crossed polarizers[8] (pseudo-null method) for the probe light allows highest accuracy in the limit of this method (±8°). In suspensions, rotational diffusion has to be taken into account and complicates the analysis. More structural information is obtainable in photoselection experiments with oriented purple membranes,[9−11] since the angle between the transition dipole moment and the membrane normal as well as the change in the azimuthal angle may be determined. All photoselection experiments suffer from an intrinsically low signal-to-noise ratio, however. Recently, we showed[12] that isotropic excitation of oriented immobilized purple membranes gets around this problem. In contrast to the photoselection experiments, which require that only an infinitesimal fraction of the chromophores

* Corresponding author. E-mail: HEYN@PHYSIK.FU-BERLIN.DE. Fax: 49-30-838-5186.

10.1021/jp990679x CCC: $18.00
Published on Web 07/09/1999

is excited, it is possible and advantageous to excite with high (nearly saturating) intensities. Information on the azimuthal angle is lost, but in this way the mathematical expression for the anisotropy is simplified substantially. A major problem remains, however: in general, the intermediates in a photocycle overlap both spectrally and kinetically. Since neither the intermediate spectra nor their relative time-dependent concentrations are exactly known, the transient anisotropy does not supply the anisotropies of the intermediates in a straightforward way. Approaches to determine the intermediate spectra and even the kinetic model provide reasonable results,[13−15] though the computational expense is very high. In general, however, the problem of finding the intermediate spectra and their concentrations is underdetermined[16] and the results are not unique.

In the present work, where we focus on the early intermediates K, L, and M, we will show that a few plausible assumptions are sufficient to solve one part of the problem analytically. For the remaining uncertainties, we make use of the additional information provided by the transient linear dichroism data. While the number of equations doubles with respect to the unpolarized measurements, the number of unknowns increases only by the number of intermediates, assuming that the anisotropy of the intermediates is constant over the main absorption band. The use of these additional equations from linear dichroism makes the problem well determined and leads to a unique solution.

In our experimental setup we improved the isotropic excitation by varying the intensities of the two exciting beams independently. We introduced a measuring scheme, which we already successfully applied to steady-state linear dichroism measurements.[17] In this method, the oriented sample is placed between two parallel polarizers. The time-dependent transmitted intensity is measured as a function of the polarization angle. In this way, polarization artifacts (due to optical elements behind the sample) are eliminated and the accuracy of the transient anisotropy is substantially improved. In addition to the transient absorption and anisotropy changes, our novel method also yields the transient birefringence changes. Using the Kramers−Kronig transform, the measured birefringence changes were shown to be in excellent agreement with the observed transient linear dichroism data. This constitutes an important control experiment and shows that the transient linear dichroism data were measured correctly.

The experimental method and formalism mentioned above were applied with oriented purple membranes to the K, L, and M intermediates of bR. In a model-independent way the relative concentrations, spectra, and anisotropies of these intermediates were determined. The angles between the transition dipole moments and the membrane normal were obtained from the anisotropies for each intermediate.

2. Materials and Methods

2.1. Preparation of Oriented PM Samples. The orientation of purple membranes in high magnetic fields and immobilization in polyacrylamide gels was performed as described.[12,17] We used a 14 T superconducting magnet and achieved an orientational order parameter S_2 of about 0.5. The oriented gel samples were prepared in a standard 4 × 10 mm quarz cuvette. The magnetic field (orientation axis) was parallel to the vertical (long) side of the cuvette. Oriented samples of the mutant D96A were prepared in the same way.

2.2. Steady-State Polarized Absorption Measurements. The steady-state measurements were performed in the flash apparatus, since the ground state data (extinction and related anisotropy) should be determined under the same experimental conditions as the time-resolved measurements. A schematic diagram of the measuring beam is shown in Figure 1. The white light emerging from the tungsten halogen lamp (LS) is focused with a condensor lens (CL) on the entrance slit (2 mm width) of the monochromator M1 (H10VIS, dispersion 8 nm/mm, Jobin-Yvon, I.S.A.). The divergent light from the exit slit (1 mm width) is collected by lens L1 and passes rather parallel through the oriented sample S (thickness 10 mm), which is placed between the two polarizers P_1 and P_2. Both polarizers are adjusted at the same polarization angle θ. θ is defined with respect to the orientation axis of the sample which coincides with the vertical (long) side of the cuvette (see Figures 1 and 2). For $\theta = 0°$ the transmission direction of the polarizer is parallel to the orientation axis. The apertures A1 and A2 cut off diverging rays. Lens L2 collimates the beam on the entrance slit (1 mm width) of the monochromator M2 (DH10VIS, dispersion 4 nm/mm, Jobin-Yvon, I.S.A.). The light emerging from M2 (exit slit width 1 mm) is detected with a photomultiplier tube (R928, Hamamatsu). The output voltage is proportional to the light intensity.

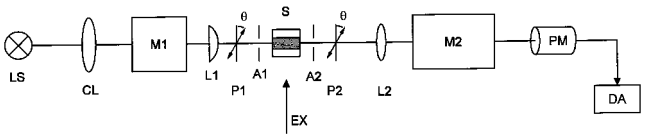

Figure 1. Experimental setup of the measuring beam: LS, light source; CL, condensor lens; M1,M2, monochromators; L1,L2; lenses; P1,P2, polarizers; A1,A2, apertures; S, sample; EX, excitation; PM, photomultiplier; DA, data acquisition. The orientation axis is perpendicular to the plane of the drawing. At $\theta = 0°$ the polarizers are parallel to the orientation axis.

We measured the transmitted intensity $I(\lambda,\theta,E_0,r_E,\Delta\phi_E)$ at at least eight polarization angles θ (−20°, 0°, 20°, 40°, 50°, 70°, 90° and 110°) and at 11 wavelengths λ (410, 460, 490, 520, 543, 570, 590, 610, 635, 650, and 670 nm) in the light-adapted state. E_0 is the isotropic extinction (absorption + scattering contribution) of the sample, r_E the related anisotropy, and $\Delta\phi_E$ the total phase difference ($\phi_{||} - \phi_{\perp}$). The choice of these special wavelengths is not essential in our experiments. Since we focus in this work on the main absorption bands of the K and L intermediates (λ_{max} at 590 and 540 nm, respectively) and the bR ground state, additional measurements at shorter wavelengths are not required. For measurements on the M intermediate with the mutant D96A, however, we used the additional wavelengths of 390 and 430 nm. The values 543 and 635 nm were picked to compare with measurements using a green He−Ne laser and a red diode laser, respectively for the measuring beam. Measurements with an identical cuvette without purple membranes provide the reference intensity ($I(\lambda, \theta, E_0 = 0, r_E = 0, \Delta\phi_E = 0)$) including correction for the lamp spectrum, the transmittance of the monochromators, and reflection losses. The scattering background was determined with an oriented sample of bleached (chromophore free) membranes.[17]

2.3. Time-Resolved Polarized Absorption Spectroscopy. The sample was excited with flashes (pulse width 10−20 ns; wavelength 532 nm) from a frequency-doubled Nd:YAG laser (Spectra Physics GCR 16). The intensity was reduced to 20 mJ/cm^2 and the beam diameter was expanded to 10−15 mm. In this way, the intensity at the sample was well below 20 mJ/cm^2. Absorption spectra were measured before and after each series of experiments which involved up to 10^4 flashes. The change in absorbance at 570 nm was at most 2%, indicating

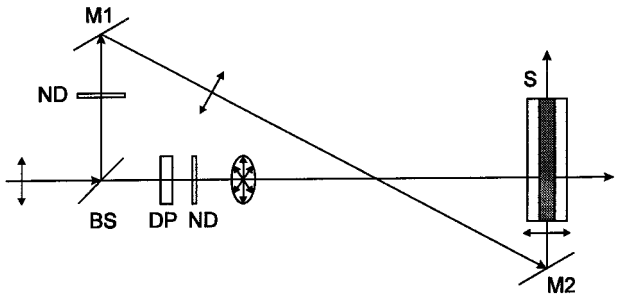

Figure 2. Excitation geometry: BS, beam splitter; M1,M2, mirrors; DP, depolarizer; ND, neutral-density filters; S, sample in 4 × 10 mm cuvette. Orientation axis parallel to long side of cuvette.

that bleaching effects as observed in ref 18 above 20 mJ/cm^2 are very minor. The absorbance changes were corrected for this small bleaching effect, when required.

The geometry for isotropic excitation is illustrated in Figure 2; the plane of the figure is perpendicular to the measuring beam. The linearly polarized beam from the laser is divided by a 50:50 beam splitter. The transmitted part is depolarized either with a (pseudo)-depolarizer or a quarter-wave plate, which causes circularly polarized light. Though the temporal and spatial distributions of the polarization are different in both cases, the effect on the sample is not substantially different. The reflected part is deflected by mirrors M1 and M2, crosses the sample from the bottom of the cuvette, and is polarized perpendicular to the transverse polarization of the transmitted part of the excitation beam (Figure 2). The relative intensities of the two beams may be varied with neutral-density filters ND, in order to equalize the intensities of the three different polarization directions. A criterion for isotropic excitation is the zero anisotropy of an isotropic sample. By varying the neutral-density filters, positive, negative, or zero anisotropy values can be set for the isotropic sample.

The data were acquired in the following way: The preamplified signal was split into two channels. The first channel was measured with a 500 MHz sampling oscilloscope (LeCroy 9350A, 8-bit resolution, 100-kbyte memory) and the second channel with an A/D converter (PC Scope T512, IMTEC, 12-bit resolution, 2-Mbyte memory). Smoothing was achieved by low-pass filters of appropriate time constants. The data were compressed and averaged by changing from the linear to a logarithmic time scale (100 data points per decade). The absorbance change $\Delta A(\lambda,\theta,t)$ is calculated directly from the signal before the flash $I(\lambda,\theta,t_0)$ and the time course of the signal after the excitation $I(\lambda,\theta,t)$.

The time-resolved measurements were performed at the same 11 or 13 wavelengths and the same polarization angles as the steady-state measurements. In order to slow the decay of the K intermediate, measurements were performed at 10 °C. To achieve a sufficiently high accumulation of the L intermediate, the pH must be in the range 4.5−7.0. The wild-type data reported in this paper were measured at pH 7. The highest accumulation of the L intermediate was achieved with the mutant D96A at pH 4.7 and 20 °C. Under these conditions, L is virtually the only intermediate about 10 μs after flash excitation.

3. Data Analysis

The steady-state measurements were analyzed with an equation which we derived previously.[17] The extinction at polarization angle θ and wavelength λ depends on the isotropic extinction E_0, the related anisotropy r_E, and the phase difference $\Delta\phi_E$ in the following way:

$$E(\lambda,\theta) = \log\frac{I(\lambda,\theta,E_0=0,r_E=0,\Delta\phi_E=0)}{I(\lambda,\theta,E_0,r_E,\Delta\phi_E)}$$

$$= E_0(1-r_E) - \log[\cos^4\theta\, 10^{-3E_0r_E} + \sin^4\theta + 2\cos^2\theta\sin^2\theta\, 10^{-3/2E_0r_E}\cos(\Delta\phi_E)] \quad (1)$$

The three wavelength-dependent parameters E_0, r_E, and $\Delta\phi_E$ are composed of absorption (A) and scattering (S) contributions:

$$E_0 = A_0 + S_0, \quad E_0r_E = A_0r_A + S_0r_S, \quad \Delta\phi_E = \Delta\phi_A + \Delta\phi_S \quad (2)$$

where A_0 is the isotropic absorption, r_A the chromophore anisotropy, S_0 the isotropic scattering, r_S the scattering anisotropy, $\Delta\phi_A$ the phase difference due to the chromophore absorption, and $\Delta\phi_S$ the phase difference due to form birefringence and intrinsic birefringence of chromophore free membranes.

Assuming only negligible changes of the scattering contributions S_0, r_S, and $\Delta\phi_S$ in the photocycle of bR, the absorbance change at polarization angle θ, wavelength λ, and time after excitation t is given by the expression which follows from eq 1:

$$\Delta A(\lambda,\theta,t) = \log\frac{I(\lambda,\theta,t_0,E_0,r_E,\Delta\phi_E)}{I(\lambda,\theta,t,E(t),r_E(t),\Delta\phi_E(t))}$$

$$= \Delta A(t)\,(1-R(t)) + \log[\cos^4\theta\, 10^{-3E_0r_E} + \sin^4\theta + 2\cos^2\theta\sin^2\theta\, 10^{-3/2E_0r_E}\cos(\Delta\phi_E)] - \log[\cos^4\theta\, 10^{-3(E_0r_E+\Delta A(t)R(t))} + \sin^4\theta + 2\cos^2\theta\sin^2\theta\, 10^{-3/2(E_0r_E+\Delta A(t)R(t))}\cos(\Delta\phi_E(t))] \quad (3)$$

$\Delta A(\lambda,t)$ is the (isotropic) absorbance change, $R(\lambda,t)$ the transient anisotropy, and $\Delta\phi_E(\lambda,t)$ the phase difference due to the transient linear birefringence. The determination of $\Delta A(\lambda,t)$, $R(\lambda,t)$, and $\Delta\phi_E(\lambda,t)$ at each wavelength λ from eq 3 requires that the parameters $E_0(\lambda)$, $r_E(\lambda)$, and $\Delta\phi_E(\lambda)$ are known from the steady state measurements. To extract information about the intermediate spectra $A_i(\lambda)$ and their anisotropies r_i ($r_i = (A_{i,\parallel} - A_{i,\perp})/(A_{i,\parallel} + 2A_{i,\perp})$) we consider $\Delta A(\lambda,t)$ and the quantity $(\Delta A(\lambda,t)R(\lambda,t))$, which is proportional to the transient linear dichroism, $LD(\lambda,t) = \Delta A_\parallel(\lambda,t) - \Delta A_\perp(\lambda,t) = 3\Delta A(\lambda,t)R(\lambda,t)$,

$$\Delta A(\lambda,t) = \sum_i (A_i(\lambda) - A_{bR}(\lambda))\, n_i(t) \quad (4)$$

$$\Delta A(\lambda,t)\, R(\lambda,t) = \sum_i (A_i(\lambda)r_i - A_{bR}(\lambda)r_{bR})\, n_i(t) \quad (5)$$

where $n_i(t)$ are the relative intermediate concentrations.

From the transient change of the phase difference $\Delta\Delta\phi(\lambda,t) = \Delta\phi_E(\lambda,t) - \Delta\phi_E(\lambda)$, we calculate the transient birefringence change

$$\Delta\Delta n(\lambda,t) = \frac{\Delta\Delta\phi(\lambda,t)}{2\pi}\frac{\lambda}{d} \quad (6)$$

which is related to the transient linear dichroism by the Kramers−Kronig transform (compare with ref 17):

$$\Delta\Delta n(\lambda,t) = \frac{3\ln 10}{2\pi^2 d} P \int_0^\infty \frac{\Delta A(\lambda',t)\, R(\lambda',t)}{(1-(\lambda'/\lambda))\,(1+(\lambda'/\lambda))}\, d\lambda' \quad (7)$$

For the determination of the intermediate spectra A_i and their anisotropies r_i, we only use the absorbance changes $\Delta A(t)$ and the transient linear dichroism ($\Delta A(t)R(t)$) according to eqs 4 and 5, since the transient birefringence change data are too noisy in the early time domain (100 ns to 10 μs). For longer times transient birefringence data of good quality can be collected and eq 7 is used to check whether the measured transient linear dichroism and the transient birefringence changes are consistent.

The time courses of the relative intermediate concentrations $n_i(t)$ are expected to be sums of exponentials for first-order kinetic schemes ($\dot{n}_i(t) = \sum K_{ij} n_j(t)$). In the photocycle of bR the number of exponentials which are required to fit the data are often larger than the number of spectroscopically distinguishable intermediates. In some cases, the number of kinetic components may be reduced, replacing two exponentials, with apparent rate constants close together, by one power law. A power law is an analytical approximation for a Gaussian distribution of first-order kinetics. We note that exponentials and power laws have the same limit for $t \to 0$ and $t \to \infty$. For further analysis the relative intermediate concentrations $n_i(t)$ can be represented as sums of a limited number of power laws (j_p) and/or exponentials (j_e):

$$n_i(t) = \sum_{j=1}^{j_p} C_{ij} \left(1 + \frac{t}{\tau_j\, n_j}\right)^{-n_j} + \sum_{j=j_p+1}^{j_p+j_e} C_{ij}\, e^{-t/\tau_j} \quad (8)$$

For the application in our formalism it makes no difference, whether we take exponentials or power laws. Inserting this expansion in eqs 4 and 5 we get

$$\Delta A(\lambda, t) = \sum_{j=1}^{j_p} B_j^A(\lambda) \left(1 + \frac{t}{\tau_j\, n_j}\right)^{-n_j} + \sum_{j=j_p+1}^{j_p+j_e} B_j^A(\lambda)\, e^{-t/\tau_j} \quad (9)$$

$$\Delta A(\lambda,t)\, R(\lambda,t) = \sum_{j=1}^{j_p} B_j^R(\lambda) \left(1 + \frac{t}{\tau_j\, n_j}\right)^{-n_j} + \sum_{j=j_p+1}^{j_p+j_e} B_j^R(\lambda)\, e^{-t/\tau_j} \quad (10)$$

where we introduce the amplitude spectra $B_j^A(\lambda)$ and $B_j^R(\lambda)$:

$$B_j^A(\lambda) = \sum_i (A_i(\lambda) - A_{bR}(\lambda)) C_{ij} \quad (11)$$

$$B_j^R(\lambda) = \sum_i (A_i(\lambda) r_i - A_{bR}(\lambda) r_{bR}) C_{ij} \quad (12)$$

The number of kinetic components $j_p + j_e$ (power laws and exponentials) might still be larger than the number of (spectroscopically distinguishable) intermediates i. For shorter notation we replace the expressions in eqs 11 and 12 by matrices assuming that the intermediate anisotropies r_i are constant over the main absorption bands:

$$\mathbf{B}^A = (\mathbf{A} - \mathbf{A}_{bR})\mathbf{C} \quad (13)$$

$$\mathbf{B}^R = (\mathbf{A}\,\mathbf{D}_i - \mathbf{A}_{bR}\,\mathbf{D}_{bR})\mathbf{C} \quad (14)$$

The row index of $\mathbf{B}^A$, $\mathbf{B}^R$, $\mathbf{A}$, and $\mathbf{A}_{bR}$ corresponds to the wavelength λ, the column index of $\mathbf{B}^A$, $\mathbf{B}^R$, and $\mathbf{C}$ to the jth component and the column index of $\mathbf{A}$, $\mathbf{A}_{bR}$ and the row index of $\mathbf{C}$ to the intermediate i. Matrix $\mathbf{A}_{bR}$ consists of identical columns. $\mathbf{D}_i$ and $\mathbf{D}_{bR}$ are diagonal matrices, with elements r_i and r_{bR}, respectively, where $\mathbf{D}_{bR} = r_{bR}\mathbf{I}$.

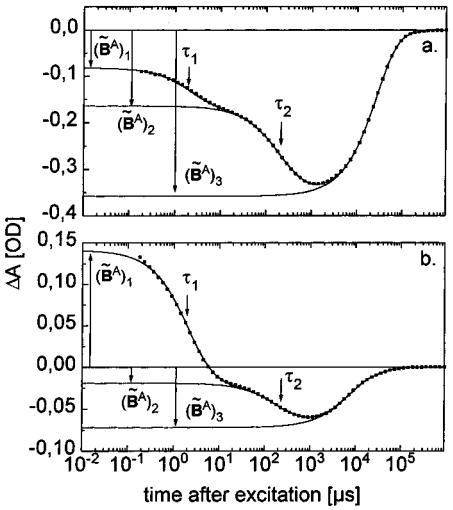

Figure 3. Illustration of the extrapolation procedure for wild type (pH 7, 50 mM KCl, 10 °C). A global fit (solid lines) was performed to the data (■) at 11 wavelengths. The fit required two power laws ($\tau_1 = 2.1$ μs, $n_1 = 3.1$, and $\tau_2 = 208$ μs, $n_2 = 2.1$) and three exponentials ($\tau_3 = 6.3$ ms, $\tau_4 = 26$ ms, $\tau_5 = 88$ ms). In (a) and (b) the data $\Delta A(\lambda,t)$ and the fits are shown for $\lambda = 570$ nm and $\lambda = 635$ nm, respectively. The arrows $(\tilde{\mathbf{B}}^A)_1$, $(\tilde{\mathbf{B}}^A)_2$, $(\tilde{\mathbf{B}}^A)_3$ represent the values of the extrapolated spectra at these wavelengths.

From the columns of $\mathbf{B}^A$, $\mathbf{B}^R$, and $\mathbf{C}$ which are arranged in order from low to high apparent time constants, we form new matrices $\tilde{\mathbf{B}}^A$, $\tilde{\mathbf{B}}^R$, and $\tilde{\mathbf{C}}$, by specified linear combinations. These linear combinations are sums of the columns, starting with index k to index $r = j_p + j_e$, which is the index of the component with the largest apparent time constant:

$$(\tilde{\mathbf{B}}^A)_k = \sum_{j=k}^{r} (\mathbf{B}^A)_j;\ (\tilde{\mathbf{B}}^R)_k = \sum_{j=k}^{r} (\mathbf{B}^R)_j;\ (\tilde{\mathbf{C}})_k = \sum_{j=k}^{r} (\mathbf{C})_j;$$
$$k = 1, .., r \quad (15)$$

The columns of $\tilde{\mathbf{B}}^A$ and $\tilde{\mathbf{B}}^R$ represent the extrapolated absorption and linear dichroism difference spectra, respectively. The columns of $\tilde{\mathbf{C}}$ contain the relative contributions of the intermediates in these difference spectra. The connection between the summing of the amplitudes and the extrapolation to $t = 0$ is obvious for $k = 1$ by considering eqs 8, 9, and 10:

$$\lim_{t\to 0} n_i(t) = \sum_{j=1}^{r} C_{ij};\quad \lim_{t\to 0} \Delta A(\lambda, t) = \sum_{j=1}^{r} B_j^A(\lambda);$$
$$\lim_{t\to 0} \Delta A(\lambda, t)\, R(\lambda, t) = \sum_{j=1}^{r} B_j^R(\lambda) \quad (16)$$

The elements of the first column of $\tilde{\mathbf{C}}$ thus are the relative intermediate concentrations n_i at $t = 0$. The first column of $\tilde{\mathbf{B}}^A$ represents the initial absorbance difference spectrum $\Delta A(\lambda,t=0)$ and the first column of $\tilde{\mathbf{B}}^R$ the initial linear dichroism difference spectrum ($\Delta A(\lambda,t=0)R(\lambda,t=0)$). Dropping successively the amplitude associated with the smallest apparent time constant generates the following extrapolated difference spectra and the related relative contributions of the intermediates. This procedure is illustrated in Figure 3 for $\Delta A(\lambda,t)$ at $\lambda = 570$ nm (a) and $\lambda = 635$ nm (b). With the columns calculated from eq 15 ($k = 1$, ..,

r), we obtain from eqs 13 and 14 the new matrix equations:

$$\tilde{\mathbf{B}}^{\mathrm{A}} = (\mathbf{A} - \mathbf{A}_{\mathrm{bR}})\tilde{\mathbf{C}} \tag{17}$$

$$\tilde{\mathbf{B}}^{\mathrm{R}} = (\mathbf{A}\,\mathbf{D}_i - \mathbf{A}_{\mathrm{bR}}\,\mathbf{D}_{\mathrm{bR}})\tilde{\mathbf{C}} \tag{18}$$

The matrices $\tilde{\mathbf{B}}^{\mathrm{A}}$ and $\tilde{\mathbf{B}}^{\mathrm{R}}$ contain the complete information about transient absorbance changes and transient linear dichroism in the bR photocycle. However, it is in general not possible to find a unique solution for the unknown elements of $\tilde{\mathbf{C}}$, **A**, and $\mathbf{D}_i$ from these equations, since the columns of $\tilde{\mathbf{B}}^{\mathrm{A}}$ and $\tilde{\mathbf{B}}^{\mathrm{R}}$ are not linearly independent. The number of linearly independent columns may be determined by singular value decomposition (SVD). For bacteriorhodopsin only three basis spectra are significant.[13,19] It is therefore necessary to reduce $\tilde{\mathbf{B}}^{\mathrm{A}}$ and $\tilde{\mathbf{B}}^{\mathrm{R}}$ to three linearly independent columns which are supposed to contain contributions of only three intermediates (with linearly independent spectra). The other columns have to be dropped. The $\tilde{\mathbf{C}}$ matrix shrinks to a square matrix of rank 3. In the following eqs 17 and 18 are to be taken as equations of the reduced matrices. A criterion for the quality of the reduced matrices is the compatibility with the SVD basis spectra **S**, i.e. there is a nonsingular transformation matrix $\mathbf{C}'$ so that $\mathbf{S} = \tilde{\mathbf{B}}^{\mathrm{A}}\tilde{\mathbf{C}}'$.

To reduce the number of unknowns, we eliminate the matrix of the intermediate spectra **A** from eqs 17 and 18. This can be done by solving eq 17 for **A**

$$\mathbf{A} = \tilde{\mathbf{B}}^{\mathrm{A}}\tilde{\mathbf{C}}^{-1} + \mathbf{A}_{\mathrm{bR}} \tag{19}$$

and inserting in eq 18, assuming all the r_i are different:

$$\tilde{\mathbf{B}}^{\mathrm{R}} = ((\tilde{\mathbf{B}}^{\mathrm{A}}\tilde{\mathbf{C}}^{-1} + \mathbf{A}_{\mathrm{bR}})\mathbf{D}_i - \mathbf{A}_{\mathrm{bR}}\mathbf{D}_{\mathrm{bR}})\tilde{\mathbf{C}} \tag{20}$$

Since $\tilde{\mathbf{C}}$ and its inverse appear in eq 20, we eliminate $\tilde{\mathbf{C}}$ by multiplication with $\tilde{\mathbf{C}}^{-1}$ from the right. Rearranging yields:

$$\tilde{\mathbf{B}}^{\mathrm{R}}\tilde{\mathbf{C}}^{-1} - \tilde{\mathbf{B}}^{\mathrm{A}}\tilde{\mathbf{C}}^{-1}\mathbf{D}_{\mathrm{i}} - \mathbf{A}_{\mathrm{bR}}(\mathbf{D}_i - \mathbf{D}_{\mathrm{bR}}) = \mathbf{0} \tag{21}$$

In this matrix equation the columns of $\tilde{\mathbf{C}}^{-1}$ are decoupled, and each column $(\tilde{\mathbf{C}}^{-1})_i$ is connected to only one intermediate anisotropy r_i. Each column $(\tilde{\mathbf{C}}^{-1})_i$ and the related anisotropy r_i have to satisfy the same vector equation:

$$(\tilde{\mathbf{B}}^{\mathrm{R}} - r_i\,\tilde{\mathbf{B}}^{\mathrm{A}})(\tilde{\mathbf{C}}^{-1})_i - (r_i - r_{\mathrm{bR}})(\mathbf{A}_{\mathrm{bR}})_i = \vec{0} \tag{22}$$

This is an underdetermined nonlinear problem in the unknowns $(\tilde{\mathbf{C}}^{-1})_i$ and r_i, i.e. the vector eq 22 consists of three linearly independent equations which contain four unknowns. Using constraints on the elements of $\tilde{\mathbf{C}}^{-1}$, so that the problem is well determined, a (locally) unique solution may be found by numerical minimization of the left side of eq 22 for each column of $\tilde{\mathbf{C}}^{-1}$ and the related anisotropy r_i.

For each column $(\tilde{\mathbf{C}}^{-1})_i$ the related spectrum $\mathbf{A}_i$ can be calculated from column *i* of the matrix eq 19:

$$(\mathbf{A})_i = \tilde{\mathbf{B}}^{\mathrm{A}}(\tilde{\mathbf{C}}^{-1})_i + (\mathbf{A}_{\mathrm{bR}})_i \tag{23}$$

As a cross check for the determination of the anisotropy r_i in the minimization procedure, we solve eq 18 for $\mathbf{AD}_i$ and consider column *i*:

$$r_i(\mathbf{A})_i = \tilde{\mathbf{B}}^{\mathrm{R}}(\tilde{\mathbf{C}}^{-1})_i + r_{\mathrm{bR}}\,(\mathbf{A}_{\mathrm{bR}})_i \tag{24}$$

We assumed above that the anisotropy is independent of the wavelength within one electronic absorption band, but in practice the right side of eq 24 is not exactly proportional to the spectrum $(\mathbf{A})_i$. The deviations from the proportionality serve as a criterion for the quality of the data. We calculate r_i as a wavelength-dependent quantity (the index λ refers to the wavelength):

$$(r_i)_\lambda = (\tilde{\mathbf{B}}^{\mathrm{R}}(\tilde{\mathbf{C}}^{-1})_i + r_{\mathrm{bR}}(\mathbf{A}_{\mathrm{bR}})_i)_\lambda/((\mathbf{A})_i)_\lambda \tag{25}$$

and compare with the weighted average value

$$\bar{r}_i = ((\mathbf{A})_i)^{-1}(\tilde{\mathbf{B}}^{\mathrm{R}}(\tilde{\mathbf{C}}^{-1})_i + r_{\mathrm{bR}}\,(\mathbf{A}_{\mathrm{bR}})_i) \tag{26}$$

where $((\mathbf{A})_i)^{-1}$ is the pseudoinverse of the spectrum. This mathematical procedure (multiplication with the pseudoinverse of $(\mathbf{A})_i$ from the left) is equivalent to an averaging procedure, where the weights are given by the squares of the absorption values:

$$\bar{r}_i = \left(\sum_\lambda (r_i)_\lambda\,((\mathbf{A})_i)_\lambda^{\,2}\right)\Big/\left(\sum_\lambda ((\mathbf{A})_i)_\lambda^{\,2}\right) \tag{27}$$

The weighted average value $\bar{r}_i$ should be identical to the value r_i determined in the minimization procedure.

The completely determined matrix $\tilde{\mathbf{C}}$ provides information about the ratio of the concentrations of the three intermediates in the extrapolated states and can be used to calculate their time courses. For this purpose we consider eqs 4 and 5 in a matrix representation:

$$\Delta\mathbf{A} = (\mathbf{A} - \mathbf{A}_{\mathrm{bR}})\mathbf{n} \tag{28}$$

$$\Delta\mathbf{AR} = (\mathbf{AD}_i - \mathbf{A}_{\mathrm{bR}}\mathbf{D}_{\mathrm{bR}})\mathbf{n} \tag{29}$$

where the rows of **n** are the time courses of the intermediates, i.e. the column index of $\Delta\mathbf{A}$, $\Delta\mathbf{AR}$, and **n** corresponds to the time *t*. From both equations **n** is calculated using $(\mathbf{A} - \mathbf{A}_{\mathrm{bR}})$ and $(\mathbf{AD}_i - \mathbf{A}_{\mathrm{bR}}\mathbf{D}_{\mathrm{bR}})$ of eqs 17 and 18 and inverting these expressions:

$$\mathbf{n} = \tilde{\mathbf{C}}\,(\tilde{\mathbf{B}}^{\mathrm{A}})^{-1}\Delta\mathbf{A} \tag{30}$$

$$\mathbf{n} = \tilde{\mathbf{C}}(\tilde{\mathbf{B}}^{\mathrm{R}})^{-1}\Delta\mathbf{AR} \tag{31}$$

$(\tilde{\mathbf{B}}^{\mathrm{A}})^{-1}$ and $(\tilde{\mathbf{B}}^{\mathrm{R}})^{-1}$ are the pseudoinverses of $\tilde{\mathbf{B}}^{\mathrm{A}}$ and $\mathbf{B}^{\mathrm{R}}$, respectively. The second equation serves as a check, whether $\tilde{\mathbf{C}}$ is consistent with both absorbance and transient linear dichroism changes over the considered time range. The time courses of the intermediates do not supply a unique kinetic model, however, since the model function for the global fitting procedure consists either of more exponentials than intermediates or of functions, such as the power laws, which do not represent the simple case of first-order kinetics.

Application to the Early Intermediates. The formalism developed so far is of general validity. For the analysis of the early intermediates, K, L, and M it is useful, however, to introduce the following two constraints on the intermediate spectra **A** and on the $\tilde{\mathbf{C}}$ matrix:

1. We assume that the fraction of cycling molecules η is conserved in the three extrapolated states, i.e. the sum of the contributions of K, L, and M in the extrapolated difference

spectra (columns of $\tilde{\mathbf{B}}^{A}$) is constant, provided that the time constants of the relaxations are sufficiently separated:

$$\sum_{i=1}^{3}\tilde{C}_{ij} = \eta \leftrightarrow \sum_{i=1}^{3}(\tilde{\mathbf{C}}^{-1})_{ij} = 1/\eta \qquad \text{for } j = 1, 2, 3 \quad (32)$$

2. Since the absorption maximum of the M intermediate is at $\lambda = 410$ nm and since the width of the M spectrum is expected to be comparable to that of bR and the other intermediates, we assume that the absorption of M is identical to zero for wavelengths larger or equal than 520 nm: $A_M(\lambda \geq 520\text{ nm}) \equiv 0$.

Taking into account the second constraint, we consider eqs 17−26 only in the wavelength region $\lambda \geq 520$ nm; i.e. we drop the rows which are related to smaller wavelengths. Hence the third column of the reduced matrix $\mathbf{A}$ corresponding to the M intermediate is the null vector $(\mathbf{A})_3 = \vec{0}$. In this way, the spectrum of the M intermediate and it's anisotropy r_M do not contribute in the further analysis. The spectra of K, L, and bR have to be linearly independent and apart from r_K and r_L the anisotropy of the bR groundstate r_{bR} may be considered as an unknown. Thanks to the constraints (1) and (2), some of the unknown parameters may be determined quasi analytically, without the nonlinear minimization procedure.

Since $(\mathbf{A})_3$ is zero, eq 23 allows to determine $(\tilde{\mathbf{C}}^{-1})_3$, the third column of $\tilde{\mathbf{C}}^{-1}$. Provided that the number of wavelength points is larger than 3, eq 23 is an overdetermined system of linear equations, for which the least-squares solution may be found by multiplication with the pseudoinverse matrix of $(\tilde{\mathbf{B}}^{A})$ from the left and rearranging:

$$(\tilde{\mathbf{C}}^{-1})_3 = -(\tilde{\mathbf{B}}^{A})^{-1}(\mathbf{A}_{bR})_3 \quad (33)$$

Using the conservation constraint (eqs 32), $(\tilde{\mathbf{C}}^{-1})_3$ provides η, the fraction of cycling molecules. Moreover, the anisotropy of the ground state r_{bR} may be determined from $(\tilde{\mathbf{C}}^{-1})_3$, considering eq 24 for $i = 3$ with $(\mathbf{A})_3 = \vec{0}$. We calculate r_{bR} as a wavelength-dependent quantity

$$(r_{bR})_\lambda = -(\tilde{\mathbf{B}}^{R}(\tilde{\mathbf{C}}^{-1})_3)_\lambda/((\mathbf{A}_{bR})_3)_\lambda \quad (34)$$

and compare with the weighted average value

$$\bar{r}_{bR} = -((\mathbf{A}_{bR})_3)^{-1}\tilde{\mathbf{B}}^{R}(\tilde{\mathbf{C}}^{-1})_3 \quad (35)$$

The value of r_{bR} is exactly identical to the steady-state anisotropy r_A only in the case of perfect isotropic excitation. If the excitation is slightly anisotropic, r_{bR} (instead of r_A) is the right ground state reference for the anisotropy of the intermediates.

Considering eqs 23, 25, and 26 not only for $\lambda \geq 520$ nm but in the full spectral range, $(\tilde{\mathbf{C}}^{-1})_3$ allows to determine the spectrum of the M intermediate, as well as the wavelength-dependent anisotropy of M and the weighted average anisotropy. It is assumed that the anisotropy of bR which we determined above for $\lambda \geq 520$ nm is the same in the short wavelength range.

In the preceding section, we only used the above constraints on the $\tilde{\mathbf{C}}$ matrix and on the spectrum of the M intermediate. By making the very reasonable assumption that only K contributes in the first extrapolated state, the problem is simplified substantially. $\tilde{\mathbf{C}}$ and its inverse $\tilde{\mathbf{C}}^{-1}$ have the following shapes:

$$\tilde{\mathbf{C}} = \begin{pmatrix} x_1 & x_2 & x_3 \\ 0 & y_2 & y_3 \\ 0 & z_2 & z_3 \end{pmatrix} \quad (36)$$

$$\tilde{\mathbf{C}}^{-1} = \frac{1}{x_1(y_2z_3 - y_3z_2)} \begin{pmatrix} (y_2z_3 - y_3z_2) & (x_3z_2 - x_2z_3) & (x_2y_3 - x_3y_2) \\ 0 & x_1z_3 & -x_1y_3 \\ 0 & -x_1z_2 & x_1y_2 \end{pmatrix} \quad (37)$$

From the conservation constraint (eq 32) it follows that x_1 is identical to the fraction of cycling molecules η. Thus, also the first column of $\tilde{\mathbf{C}}^{-1}$ is determined and the spectrum of the K intermediate follows from eq 23. The wavelength-dependent anisotropy of K is given by eq 25 and the weighted average anisotropy by eq 26.

The spectrum of the L intermediate and its anisotropy cannot be derived in this quasi analytical way, since the second column of the $\tilde{\mathbf{C}}^{-1}$ matrix is independent from the first and the third column. This column and the related anisotropy r_L may be determined by numerical minimization of the left side of eq 22, using the conservation constraint eq 32. In order to find a linearly independent solution in the minimization procedure, it is advantageous to express the elements of the second column of $\tilde{\mathbf{C}}^{-1}$ in terms of the elements of the second column of the $\tilde{\mathbf{C}}$ matrix and the elements of the third column of $\tilde{\mathbf{C}}^{-1}$, which are explicitly determined above (eq 33). Using the second column of the matrix relation $\tilde{\mathbf{C}}^{-1}\tilde{\mathbf{C}} = \mathbf{I}$ we get

$$(\tilde{\mathbf{C}}^{-1})_{12} = \left(-\frac{1}{\eta}x_2 - (\tilde{\mathbf{C}}^{-1})_{13}z_2\right)/y_2 \quad (38)$$

$$(\tilde{\mathbf{C}}^{-1})_{22} = (1 - (\tilde{\mathbf{C}}^{-1})_{23}\,z_2)/y_2 \quad (39)$$

$$(\tilde{\mathbf{C}}^{-1})_{32} = -(\tilde{\mathbf{C}}^{-1})_{33}z_2/y_2 \quad (40)$$

where x_2, y_2, and z_2 have to obey the conservation constraint eq 32. We note that the elements of $\tilde{\mathbf{C}}$ are positive by definition, while this is not the case for $\tilde{\mathbf{C}}^{-1}$. Thus, the variation of the positive parameters x_2, y_2, and z_2 instead of $(\tilde{\mathbf{C}}^{-1})_{12}$, $(\tilde{\mathbf{C}}^{-1})_{22}$, and $(\tilde{\mathbf{C}}^{-1})_{32}$ in the minimization procedure guarantees physically relevant results. It is also useful to consider the relationship between x_2 and x_3, which results directly from the identity $\tilde{\mathbf{C}}\tilde{\mathbf{C}}^{-1} = \mathbf{I}$:

$$\eta(\tilde{\mathbf{C}}^{-1})_{13} + x_2(\tilde{\mathbf{C}}^{-1})_{23} + x_3(\tilde{\mathbf{C}}^{-1})_{33} = 0 \quad (41)$$

Since x_2 and x_3 have to take on positive values, eq 41 provides a lower limit either for x_2 or for x_3, if $(\tilde{\mathbf{C}}^{-1})_{13} \neq 0$. From the second column of $\tilde{\mathbf{C}}^{-1}$ we calculate the spectrum of L, $(\mathbf{A})_2$, according to eq 23. The wavelength-dependent anisotropy of L is given by eq 25 and the weighted average anisotropy by eq 26 for $i = 2$.

4. Results

4.1. Dependence on the Polarization Angle. The polarized absorbance data $\Delta A(\lambda,\theta,t)$ were further compressed and averaged in time, so as to have 10 data points per decade. As an example and to illustrate the significant contribution of linear birefringence changes to the signal, the polarized absorbance changes at $\lambda = 635$ nm are presented in the contour plot of Figure 4a. While the maximum is located at 90° ($t \approx 150$ ns), the minimum appears around 60° in the time range of $t \approx 1$ ms. The angular dependence of the data was fitted with eq 3 at each time t and each measured wavelength λ. The residuals for the fit at $\lambda = 635$ nm are presented in the contour plot of Figure 4b. The residuals are at most ±2.5 m OD in the early time domain, and decrease with increasing time, since the signal-

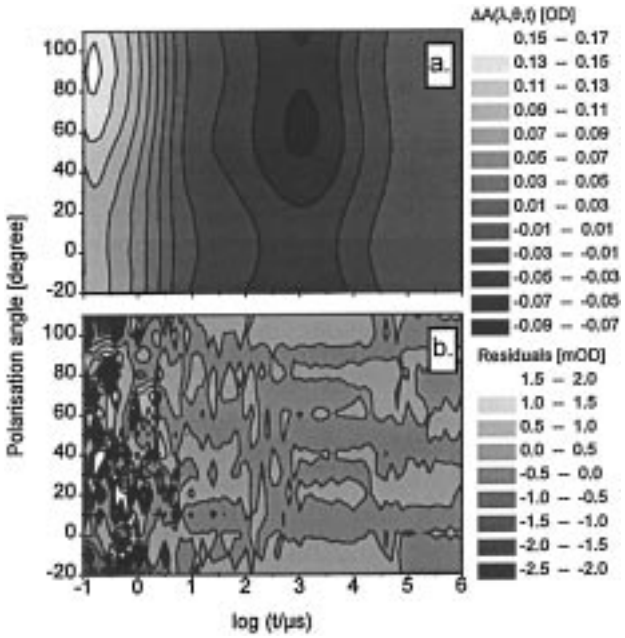

Figure 4. Contour plot of the polarized absorbance change $\Delta A(\lambda,\theta,t)$ for wild type (pH 7, 50 mM KCl, 10 °C) at $\lambda = 635$ nm: (a) data; (b) residuals of the fits of the data with eq 3.

to-noise ratio increases due to the averaging procedure. Figure 5 shows the dependence on the polarization angle at $\lambda = 635$ nm at four selected time points ($t = 140$ ns, 14 μs, 1.4 ms, 14 ms). The continuous curve through the data points shows the excellent fit with eq 3. At $t = 140$ ns the polarized absorbance change $\Delta A(\lambda,\theta,t)$ is a monotonic function of the polarization angle θ for $0^\circ \leq \theta \leq 90°$, i.e. the relative contribution of the linear birefringence change is small. At $t = 14$ μs, 1.4 ms, and 14 ms, there is a minimum near 60°, which is due to a larger relative contribution of the linear birefringence change, corresponding to phase changes $\Delta\Delta\phi$ up to 6°. The dashed curves show the predicted dependence in the absence of linear birefringence changes, i.e., with $\Delta\Delta\phi(t) = 0°$. The contribution of linear birefringence changes to the signal is clearly substantial.

4.2. Resulting Time Traces. The results from the angular fits for $\Delta A(\lambda,t)$, $\Delta A(\lambda,t)$ $R(\lambda,t)$, and $\Delta\Delta n(\lambda,t)$ are shown in Figure 6, where only five wavelengths are selected. Since the traces of the absorption changes $\Delta A(\lambda,t)$ (Figure 6a) and the transient linear dichroism $\Delta A(\lambda,t)$ $R(\lambda,t)$ (Figure 6b) seem to be proportional at first sight, we also present the transient anisotropy $R(\lambda,t)$ in Figure 6c. The singularities arise of course from the zeros of $\Delta A(\lambda,t)$. An exact quantitative interpretation of these time traces is not possible, due to the fact that neither the spectra of the intermediates nor the kinetic model are exactly known. Some features of the intermediate anisotropies, but not their precise values, emerge, however, from the time traces. (1) Except for the 410 nm curve all traces reach approximately -0.15 at $t \approx 1$ ms (box 1, Figure 6c), which should to be close the groundstate anisotropy r_{bR}. The smaller absolute value of the 410 nm−trace in this time domain (box 1), together with $\Delta A(410\text{ nm}, 1\text{ ms}) > 0$, indicates, that the absolute value of the M-anisotropy is smaller ($r_M \approx -0.135$) than the groundstate anisotropy. (2) The same argument holds for the K intermediate, considering the time domain $t = 200$ ns to 2μs of the 635 nm traces (box 2). (3) For the L intermediate we consider the traces for 490, 520, and 570 nm at $t = 10$ μs (boxes 3):

$$R(490\text{ nm}, 10\ \mu\text{s}) \ll r_{bR} < R(570\text{ nm}, 10\ \mu\text{s}) \ll R(520\text{ nm}, 10\ \mu\text{s})$$

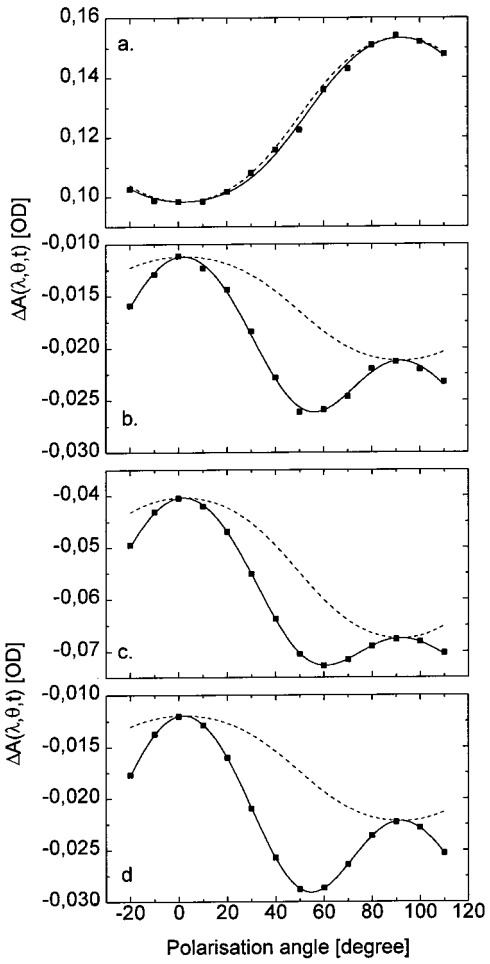

Figure 5. Sections of the polarized absorption data from Figure 4 ($\lambda = 635$ nm) at four time points: (■) data; solid lines, best fit with eq 3; dashed lines, predicted dependence in the absence of linear birefringence. (a) $t = 140$ ns, (b) $t = 14$ μs, (c): $t = 1.4$ ms, (d) $t = 14$ ms.

$$\Delta A(490\text{ nm}, 10\ \mu\text{s}) > 0 > \Delta A(520\text{ nm}, 10\ \mu\text{s}) \gg \Delta A(570\text{ nm}, 10\ \mu\text{s})$$

Assuming that the L contribution prevails in this time domain, the transient anisotropy (see eqs 4 and 5) simplifies to $R = (A_L r_L - A_{bR} r_{bR})/(A_L - A_{bR})$ and the above inequalities lead to the conclusion, that $0 > r_L > r_{bR}$.

The linear birefringence changes (Figure 6d) are quite noisy in the first two time decades. In the time domain $t > 10$ μs, however, data of good quality were obtained (Figure 6d). The transient linear dichroism data were transformed via the Kramers−Kronig transform, according to eq 7. In Figure 7 the linear birefringence calculated in this way is compared with the observed linear birefringence for $t = 14$ μs (little M) and $t = 2.3$ ms (mostly M), for the mutant D96A. The reason for using the mutant data is simply that for the mutant more wavelengths were used in the UV than for wild type, which leads to better results in the millisecond time range when M accumulates ($\lambda_{max} = 410$ nm). The numerical calculations have been carried out, by using the spline fits on the linear dichroism data (Figure 7a). In Figure 7b the Kramers−Kronig transforms of the linear dichroism data from Figure 7a (lines) are compared with the observed transient birefringence data (symbols). No scaling factor was used. The agreement is excellent. The deviation for $t = 2.3$ ms at $\lambda < 410$ nm is simply due to the lack of transient linear dichroism data at shorter wavelengths. Similar agreement was observed for wild type.

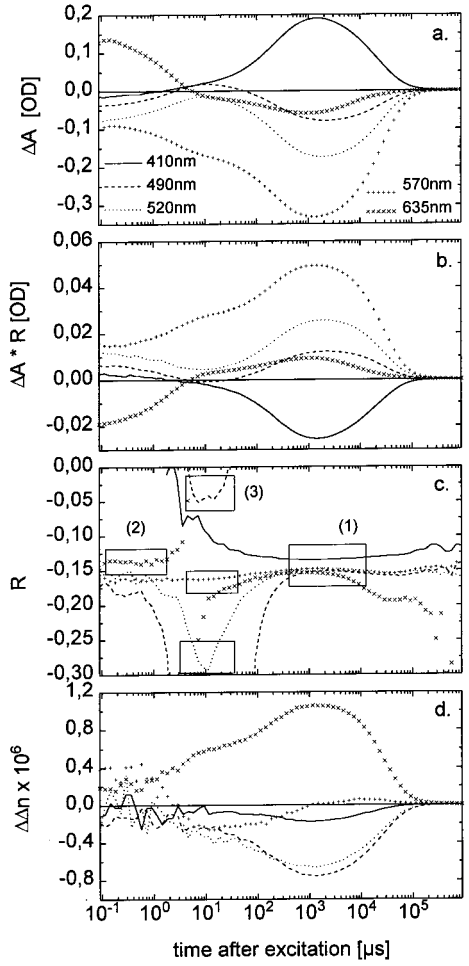

Figure 6. Results of the angular fits (five wavelengths selected): $\lambda =$ 410, 490, 520, 570, and 635 nm. Data for wild type, same conditions as in Figure 4. (a): $\Delta A(\lambda,t)$, isotropic absorbance changes; (b) ($\Delta A(\lambda,t)$ $R(\lambda,t)$), transient linear dichroism; (c) $R(\lambda,t)$ anisotropy calculated from (a) and (b); (d) $\Delta\Delta n(\lambda,t)$, linear birefringence changes.

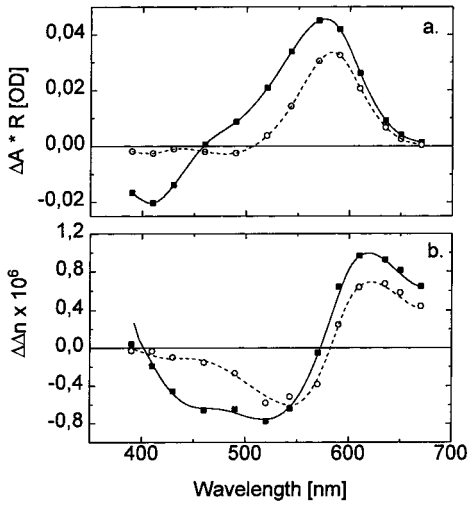

Figure 7. Relation between transient linear dichroism and linear birefringence changes. Data for the mutant D96A, pH 4.7, 50 mM KCl, 20 °C. (a) Symbols: transient linear dichroism data at $t = 14$ μs (○) and $t = 2.3$ ms (■), respectively. Lines: Spline fits of the data. (b) Symbols: data of the linear birefringence changes. Lines: Kramers−Kronig transform of the spline fits in (a).

4.3. Intermediate Spectra and Intermediate Anisotropies from the Superimposed Amplitude Spectra. For the further analysis we only use the absorption changes $\Delta A(\lambda,t)$ and the transient linear dichroism $\Delta A(\lambda,t)R(\lambda,t)$, since the linear birefringence changes $\Delta\Delta n(\lambda,t)$ are too noisy in the early time domain and do not supply additional information. The time traces ($\Delta A(\lambda,t)$ and $\Delta A(\lambda,t)R(\lambda,t)$) were fitted globally with appropriate model functions, according to eqs 9 and 10. We checked various combinations of power laws and exponentials and found, that the best fit with a minimal number of parameters was achieved with two power laws ($\tau_1 = 2.1$ μs, $n_1 = 3.1$ and $\tau_2 = 208$ μs, $n_2 = 2.1$) and three exponentials ($\tau_3 = 6.3$ ms, $\tau_4 = 26$ ms, $\tau_5 = 88$ ms). A higher number of power laws or exponentials or replacement of the two power laws by three or even four exponentials yields no substantial improvement. The quality of the global fit is illustrated in Figure 3 for $\lambda = 570$ nm and $\lambda = 635$ nm. The resulting amplitude spectra $B_j^A(\lambda)$ and $B_j^R(\lambda)$ are plotted in Figure 8a and b, respectively.

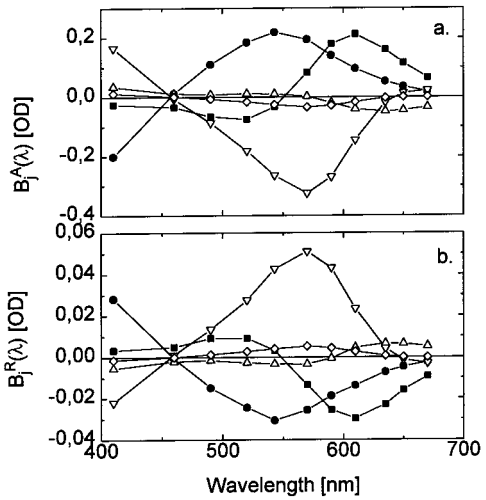

Figure 8. Results of the global fit of $\Delta A(\lambda,t)$ and ($\Delta A(\lambda,t)$ $R(\lambda,t)$) with two power laws (■, $\tau_1 = 2.1$ μs, $n_1 = 3.1$; ●, $\tau_2 = 208$ μs, $n_2 = 2.1$) and three exponentials (△, $\tau_3 = 6.3$ ms; ▽, $\tau_4 = 26$ ms, ◇, $\tau_5 = 88$ ms). Data for wild type, same conditions as in Figure 4. (a) $B^A{}_j(\lambda)$, amplitude spectra of the isotropic absorbance changes, (b), $B^R{}_j(\lambda)$, amplitude spectra of the transient linear dichroism.

In the next step, we sum over the amplitudes at each wavelength, which corresponds to linear combinations of the columns of $\mathbf{B}^A$ and $\mathbf{B}^R$, according to eq 15. For the first combination ($k = 1$), we sum over all amplitudes ($j = 1, ..., 5$), for the second ($k = 2$) we drop the first ampltitude ($j = 2, ..., 5$), and for the third ($k = 3$) only the last three amplitudes contribute ($j = 3, ..., 5$). See Figure 3 for an illustration of this extrapolation procedure at $\lambda = 570$ nm and $\lambda = 635$ nm. The resulting columns of matrices $\tilde{\mathbf{B}}^A$ and $\tilde{\mathbf{B}}^R$, the asymptotic difference spectra are shown in Figure 9a,b and the related anisotropies $(\tilde{\mathbf{R}})_k = (\tilde{\mathbf{B}}^R)_k/(\tilde{\mathbf{B}}^A)_k$ in Figure 9c. The compatibility of the columns of $\tilde{\mathbf{B}}^A$ with the SVD basis spectra, calculated from $\Delta A(\lambda,t)$ in the time range 200 ns $\leq t \leq$ 1.2 ms, was checked. This was carried out by minimization of the left side of $\mathbf{S} - \tilde{\mathbf{B}}^A\tilde{\mathbf{C}}' = \mathbf{O}$. At the minimum, e.g. with the transformation matrix $\mathbf{C}'$ which fits best this equation, the deviations were smaller than 2 mOD.

In order to calculate the $\tilde{\mathbf{C}}$ matrix, the rows in $\tilde{\mathbf{B}}^A$ and $\tilde{\mathbf{B}}^R$, which correspond to wavelengths $\lambda < 520$ nm, have to be dropped. Using eq 33 we get the third column of the $\tilde{\mathbf{C}}^{-1}$ matrix:

$$(\tilde{\mathbf{C}}^{-1})_{13} = 0.13; \quad (\tilde{\mathbf{C}}^{-1})_{23} = -0.67; (\tilde{\mathbf{C}}^{-1})_{33} = 2.92$$

According to eq 32 this column directly yields $\eta = 0.420$, the fraction of cycling molecules. We reach in our experiments such a high value due to the isotropic excitation. The average

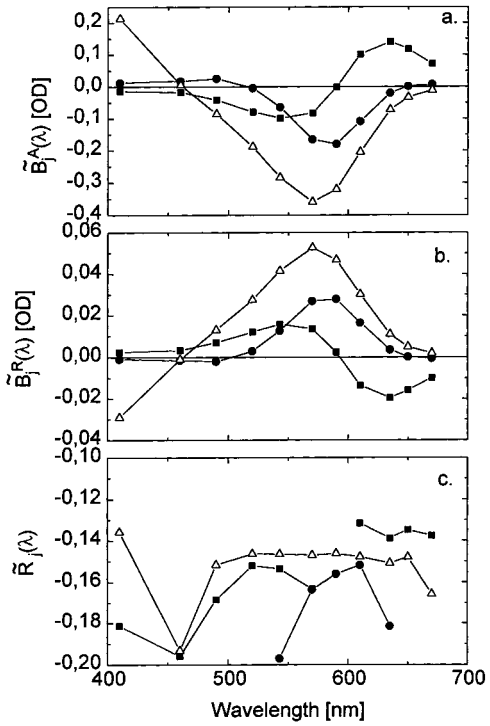

Figure 9. Asymptotic difference spectra obtained by summation of the columns of the amplitude spectra of Figure 8 according to eq 15: (a) $\tilde{B}_k^A(\lambda)$, (b) $\tilde{B}_k^R(\lambda)$, (c) $\tilde{R}_k(\lambda)$, calculated from (a) and (b). (■) $k = 1$, (●) $k = 2$, (△) $k = 3$.

anisotropies of the bR ground state and the K state are $\bar{r}_{bR} = -0.145 \pm 0.001$ and $\bar{r}_k = -0.140 \pm 0.001$, according to eqs 35 and 26. Since $(\tilde{\mathbf{C}}^{-1})_{13} > 0$ and $(\tilde{\mathbf{C}}^{-1})_{23} < 0$, eq 41 provides a lower limit for the contribution of K in the second column of $\tilde{\mathbf{B}}^A$: $x_2 \geq 0.082$. The remaining indefiniteness (intrinsically two free parameters, i.e., y_2 and z_2) is eliminated by the numerical calculations, according to eq 22 using the relations of eqs 38, 39, and 40: $x_2 = 0.082$, $x_3 = 0.0$, $y_2 = 0.338$, $y_3 = 0.077$, $z_2 = 0.0$, $z_3 = 0.343$, $r_L = -0.132$. Using these values $\tilde{\mathbf{C}}^{-1}$ was calculated. With the help of eq 26 we obtained in this way $\bar{r}_L = -0.132 \pm 0.002$, which is consistent with r_L from the minimization procedure.

The anisotropy of the M intermediate was calculated only at the wavelength of maximal absorption $\lambda = 410$ nm, assuming that the anisotropies of bR and L in the higher absorption band are the same as in the main absorption band (for evidence from steady-state measurements (see ref 17). Nevertheless, to be on the safe side, we did not make use of the data for $\lambda < 520$ nm in the above minimization procedure. Considering the relative contributions of bR, L, and M in the third column of $\tilde{\mathbf{B}}^R$, we get $r_M = -0.139$, compared with $R(410\text{ nm}, 1\text{ ms}) = -0.135$ from the time traces.

From the completely determined $\tilde{\mathbf{C}}$ matrix, we calculate the intermediate spectra (Figure 10a), using eq 19 and the related wavelength-dependent anisotropies (Figure 10b), using eqs 34 and 25. These anisotropies should be compared with the average values (horizontal lines in Figure 10b), according to eq 35 and 26. We note that the averaging is performed according to eq 27, i.e., the weighting is with $(A_i(\lambda))^2$. The anisotropies of the intermediates, which have been calculated as wavelength-dependent quantities, are very close to the average values over the main absorption bands and show only small variation over the wavelength. This validates our initial assumption in the data analysis that the anisotropies r_i are independent of λ. We can now calculate the angle θ_i between the transition dipole moment

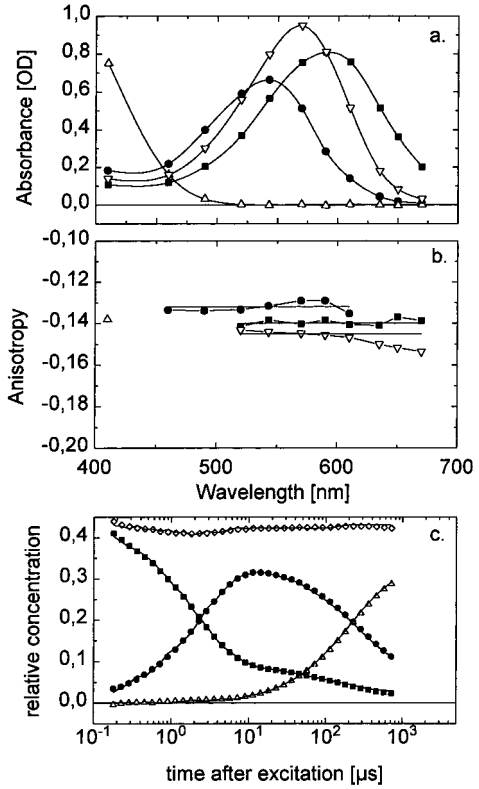

Figure 10. Results of the data analysis for wild type (same conditions as in Figure 4). (■) K, (●) L, (△) M, (▽) bR. (a) Intermediate spectra, (b) anisotropies, (c): time courses. The solid lines in (a) are spline fits. The horizontal lines in (b) are the average anisotropies $\bar{r}_i$ according to eqs 26 and 35. The symbols in (c) represent the time course calculated from the isotropic absorbance changes according to eq 30. The solid lines in (c) were calculated from the transient linear dichroism according to eq 31. ◇ in (c): sum of the relative concentrations of K, L, and M.

in the state i and the membrane normal from $r_i = S_2 P_2(\cos \theta_i)$. Since we do not know S_2 exactly we determine it from the known angle θ_{bR} and the groundstate anisotropy $r_{bR} = -0.145$. Furthermore, we make the reasonable assumption that S_2 is the same in every intermediate. With $\theta_{bR} = 70°$,[20,21] the average anisotropies of K, L, and M lead to $\theta_K = 69.3° \pm 0.3°$, $\theta_L = 68.3° \pm 0.3°$, and $\theta_M = 69.2° \pm 0.5°$.

From the $\tilde{\mathbf{C}}$ matrix, which we determined above, we get the time courses of the intermediates, i.e. the time-dependent relative concentrations of the intermediates (Figure 10c), according to eqs 30 and 31. There are only small deviations between the calculations from the isotropic absorbance changes (symbols) and the transient linear dichroism (solid lines). In both cases the sum over the concentrations of K, L, and M is very close to $\eta = 0.42$ from $t = 200$ ns to $t = 1$ ms, which is a further criterion for the validity of the analysis (compare with ref 14). The intermediate spectra and time courses (Figure 10a,c) are as expected for wt-bR under our experimental conditions (see discussion).

4.4. Experiments with the Mutant D96A. Analogous experiments were performed with the mutant D96A under various experimental conditions. In this mutant aspartate 96, the internal donor for the reprotonation of the Schiff base in the decay of M is replaced by alanine. As a result of this removal of the proton donor the decay of M is slowed by 2 orders of magnitude at neutral pH.[22] Moreover the decay of K is accelerated, so that L accumulates to a larger extent than in wild type. Thus, this mutant is appropriate to obtain better data for the anisotropies in L and M.

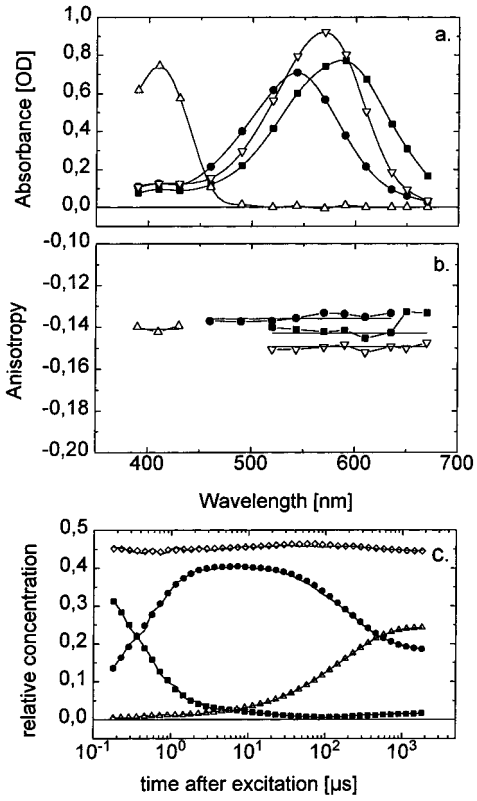

Figure 11. Results of the data analysis for D96A (same conditions as in Figure 7). (■) K, (●) L, (△) M, (▽) bR; ◇ in (c): sum of the relative concentrations of K, L, and M. For further details see legend of Figure 10.

Experiments were performed under three sets of experimental conditions: (1) pH 7, 20 °C, (2) pH 4.7, 20 °C, (3) pH 4.7, 10 °C. Under conditions (1) the decay time of M is in the seconds range and the time trace of the anisotropy at 410 nm shows a constant anisotropy from approximately 100 μs to 1 s (data not shown). These data thus do not provide any evidence for two M states with different anisotropies (early and late; pre- and postswitch) in this time range. Under conditions (2), M decays faster, allowing more extensive measurements at more wavelengths and polarization angles. In particular, to get better results for the spectrum and anisotropy of M, three wavelengths near the absorption maximum of M were included in the analysis (390, 410, and 430 nm). Measurements and data analysis were performed as described above in detail for wild type. The results are presented in Figure 11 (conditions (2)). The spectra for bR, K, and L (Figure 11a) are very close to those presented in Figure 10a for wild type. Moreover, a clear maximum in the spectrum for M can be discerned. The anisotropies in Figure 11b show the same pattern and sequence as in Figure 10b for wild type. The main difference is that better data are obtained for M and L. The average anisotropies are $r_K = -0.143 \pm 0.003$, $\bar{r}_L = -0.136 \pm 0.002$, $\bar{r}_M = -0.141 \pm 0.001$, and $r_{bR} = -0.150 \pm 0.001$. The absolute values are slightly larger than for wild type. This is due to a correspondingly larger order parameter in the sample of the mutant. Figure 11b confirms that the anisotropies of the intermediates are to a very good approximation constant across the absorption bands. Deviations occur only for K and only at the two highest wavelengths (650 and 670 nm). As Figure 11c shows, K decays rapidly. Moreover, at these two wavelengths the absorbance is already low. Accordingly, the errors in these two anisotropies for K are large. The time courses in Figure 11c show that due to the rapid decay of K, L accumulates more than in wild type and is the major species around 10 μs (compare Figure 11c with Figure 10c for wild type). Figure 11c shows that the sum of the concentrations of K, L, and M is constant over the time range considered, as required in our analysis. The same analysis was also carried out under conditions (3) in which the K intermediate is slowed, allowing better data for this intermediate. The spectra and anisotropies for D96A are under all three conditions very similar and almost identical to those of wild type. Thus in every case the sequence of anisotropies is $r_{bR} < r_K < r_M < r_L$. The corresponding angles are tabulated in Table 1.

TABLE 1: Changes of the Transition Dipole Moment (in deg) with Respect to Membrane Normal under Various Conditions ($\Delta\theta_i = \theta_i - \theta_{bR}$, Assuming $\theta_{bR} = 70°$)

	wild type pH 7, 10 °C	D96A pH 7, 20 °C	D96A pH 4.7, 20 °C	D96A pH 4.7, 10 °C
$\Delta\theta_K$	-0.7 ± 0.3	-0.9 ± 0.7	-0.9 ± 0.5	-0.9 ± 0.5
$\Delta\theta_L$	-1.7 ± 0.3	-2.0 ± 0.2	-1.7 ± 0.3	-1.6 ± 0.2
$\Delta\theta_M$	-0.8 ± 0.5	-1.3 ± 0.2	-1.1 ± 0.2	-1.1 ± 0.5

5. Discussion

5.1. Linear Birefringence Changes. We determined transient birefringence changes in the photocycle of bacteriorhodopsin from time-resolved absorption spectroscopy with linearly polarized light. Analogous to our steady-state linear birefringence measurements,[17] we measured the transmission of an oriented purple membrane sample in between two parallel polarizers after isotropic and nearly saturating excitation. In the case of perfect isotropic excitation, the orientational distribution of the excited bR molecules equals the permanent distribution of the molecules in the preoriented membranes. The signal in our measurements $\Delta A(\lambda,\theta,t)$ depends on the cosine of the total phase difference $\Delta\phi_E(t)$ (see eq 3), which is mainly due to the permanent linear birefringence of the sample $\Delta\phi_E$ and which is considerably larger than the transient change of the phase difference $\Delta\Delta\phi(t)$. The highest sensitivity would be reached at $\Delta\phi_E = \pm 90°$, $\pm 270°$, but even the permanent phase differences of $\approx 15°-45°$ in our measurements allow accurate determination of the birefringence changes for $t \geq 10$ μs. Since our method only requires an additional polarizer in the measuring beam, a spectral range at discrete wavelengths from 390 to 670 nm is available. The photoselection method[23] is about equally sensitive but uses on the other hand a retardation plate, which is specified for a particular wavelength. The adjustment of the additional polarizer in our method is relatively uncritical ($\pm 0.5°$ relative to the first polarizer has nearly no influence on the signal), while the exact orientation of the retardation plate is essential in the photoselection method. In the latter method, the information on the refractive index change was obtained from measurements at four angles of the retardation plate axis, spaced by only 0.5°. Another advantage of our method is the exact formal description, which was verified by the fits of the dependence on the polarization angle, measured at 14 angles (see Figure 5). In contrast, the expressions given in ref 23 hold only in the case of weak excitation (small absorbance changes, which is also a condition for a sufficiently high value of the anisotropy), and require the smallness of angles (phase difference and orientation of the retardation plate axis with respect to the polarizers). The spectral dependence of the linear birefringence changes in our measurements (Figure 7) shows excellent agreement with the calculations from transient linear dichroism using the Kramers−Kronig transform of eq 7. The validity of this spectral relationship for purple membranes has already been shown,[24] but our method provides higher accuracy and requires no normalization. While the interferometric method is limited to photostationary states,[24]

the time-resolved method presented here provides transient birefringence changes from $t = 10\ \mu$s to the completion of the photocycle.

5.2. Intermediate Spectra and Kinetics. In this study, we presented a matrix formalism which provides information on the intermediate spectra and their transient concentrations in the first half of the bR photocycle. The fitting procedure of the time traces and summation of the amplitudes are helpful tools in the analysis, corresponding to a smoothing and reduction of the data. In this way, we introduced the matrix $\tilde{\mathbf{C}}$, whose elements are the relative contributions of the intermediates K, L, and M in the extrapolated mixed states. We note that these elements do not represent the relative intermediate concentrations at any time t.

We use the constraints that (1) the M intermediate does not contribute to absorption for wavelengths greater or equal 520 nm, (2) the fraction of cycling molecules is conserved at least in the first half of the photocycle, and (3) in the first column of $\tilde{\mathbf{B}}^{\mathrm{A}}$ only the K intermediate contributes. With these physically plausible constraints, some of the unknown parameters may be obtained quasi analytically from the isotropic transient absorbance changes $\tilde{\mathbf{B}}^{\mathrm{A}}$. The fraction of cycling bR molecules η is determined explicitly. The remaining unknown parameters (x_2,x_3,y_2,y_3,z_2,z_3) have to obey four independent constraints, e.g. there are only two free intrinsic parameters. The range of these parameters is again restricted, since no negative absorption values and no negative contributions (x_2,x_3,y_2,y_3,z_2,z_3) are allowed. Within the relatively small parameter range, set by these inequalities, a locally unique solution was calculated numerically using both the transient absorption and the transient linear dichroism data.

In principle, our analysis should also work with the SVD basis spectra determined from $\Delta A(\lambda,t)$ and ($\Delta A(\lambda,t)\ R(\lambda,t)$), but the formalism with the $\tilde{\mathbf{C}}$ matrix provides considerable simplification of the problem. Comparing the representations of the difference spectra

$$(\mathbf{A} - \mathbf{A}_{\mathrm{bR}}) = \mathbf{S}\mathbf{X}^{-1} \quad \text{and} \quad (\mathbf{A} - \mathbf{A}_{\mathrm{bR}}) = \tilde{\mathbf{B}}^{\mathrm{A}}\tilde{\mathbf{C}}^{-1}$$

in the two formalisms, all the elements of the transformation matrix $\mathbf{X}$ are in general different from zero, while $\tilde{\mathbf{C}}$ has two zero elements in the first column due to the plausible assumption that only K contributes to the first extrapolated difference spectrum, i.e., the first column of $\tilde{\mathbf{B}}^{\mathrm{A}}$ and $\tilde{\mathbf{B}}^{\mathrm{R}}$, respectively.

The spectra $A_{\mathrm{i}}(\lambda)$ of the intermediates K, L, and M at 11 wavelengths, which emerge from our analysis, are in good agreement with the intermediate spectra determined recently,[15] based on OMA data (data acquisition with an optical multichannel analyzer). For example for wild-type we found $\lambda_{\max}$ values of 590 and 542 nm for the K and L intermediates, respectively. Figure 12a shows the good agreement between our spectra for wild type and reference spectra from OMA experiments.[15] For the L intermediate there is a small discrepancy in the amplitude ($\epsilon_{\max}$). The spectral shape is the same as in ref 15. Our spectra for the mutant D96A are compared in Figure 12b with recent results from the literature for D96N.[13,14] The agreement is clearly excellent. This result thus also validates our data analysis. In comparison with our experimental method (time traces at single wavelengths), the spectral information of the data is higher in the OMA measurements, but the accuracy in time is lower. Since we measured the angular dependence of the absorbance changes, we are able to extract the isotropic absorbance changes from our data. In this way, polarization artifacts are completely eliminated, which is not guaranteed in measurements at only one polarization angle, not even at the magic angle.[25]

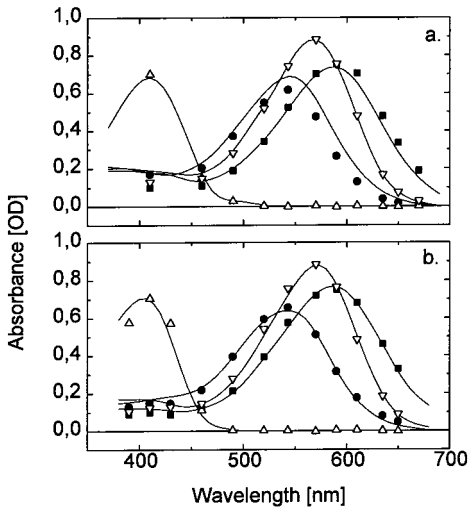

Figure 12. Comparison of the intermediate spectra from this work (■) K, (●) L, (△) M, (▽) bR) for (a) wild type (pH 7, 50 mM KCl, 10 °C) and (b) the mutant D96A (pH 7, 50 mM KCl, 20 °C) with recent literature values (solid curves). The reference spectra for wild type are from ref 15, for D96N from ref 13 (L, M, bR) and from ref 14 (K).

In contrast to the filter method[13] or the Monte Carlo search,[15] where numerous weak restricting criteria have to be implemented, we only require the three simple physically plausible constraints mentioned at the beginning of this section. With these strong constraints we get a quasi analytical solution, with only two intrinsic unknowns in a restricted range (no negative contributions and no negative extinction coefficients are allowed) remaining. The grid search or Monte Carlo search with a larger number of weak constraints will provide the best solution, which possibly depends on the minimization criterion, i.e. the weighting of the constraints. We emphasize that a mathematically unique solution does not emerge from the isotropic transient difference spectra alone.

Polarized measurements supply additonal independent information, provided that the anisotropies of the intermediates are not degenerate. In the case of complete degeneracy the transient linear dichroism and the transient absorbance changes would be proportional, i.e. the $\tilde{\mathbf{B}}^{\mathrm{A}}$ and $\tilde{\mathbf{B}}^{\mathrm{R}}$ are proportional too. In the case of nondegeneracy, the absorbance of the intermediates may be eliminated from the equations. It is not possible to find an analytical solution, however, since the problem is now nonlinear in the unknown variables. Numerical minimization yields the remaining unknown coefficients of $\tilde{\mathbf{C}}^{-1}$ and the related anisotropies. We note that the anisotropies of bR and the intermediates K, L, and M are nondegenerate (Figures 10b and Figure 11b), but do not differ much.

In this context, it is of interest to discuss another approach, which makes use of the invariance of the spectra with temperature.[16] In our notation this would mean that $\tilde{\mathbf{B}}^{\mathrm{A}}$ and $\tilde{\mathbf{C}}$ are temperature dependent, while ($\mathbf{A} - \mathbf{A}_{\mathrm{bR}}$) is temperature independent. Without constraints on the $\tilde{\mathbf{C}}$ matrix, the problem would be underdetermined, even if data at more than three temperatures are available. Using the restriction that the fraction of cycling molecules is conserved in the first half of the photocycle and that only the K intermediate contributes to the first asymptotic difference spectrum, the problem would be well determined with data at three temperatures. But it should be mentioned that this approach requires that the microscopic rate constants have different temperature dependencies. Moreover, a serious experimental problem is that at higher temperatures

(i.e., 40 °C) the decay of the K intermediate is accelerated to such an extent that the time resolution is not sufficient for the extrapolation to the initial state, corresponding to the first column in matrix $\tilde{\mathbf{B}}^{A}$. Previous simulations showed[16] that the fitting procedure is extremely sensitive to noise. The determination of intermediate spectra from absorption data at three or more temperatures using this approach was to our knowledge until now not successful. In our opinion, the analysis of data from linear dichroism measurements, assuming constant anisotropies of the intermediates over the main absorption bands, is a more promising approach to determine the intermediate spectra in the photocycle of bacteriorhodopsin.

5.3. Anisotropies of the Intermediates and Reorientation of the Transition Dipole Moment. In this study we determined the anisotropies r_i and calculated from them the angles of the transition dipole moment with respect to the membrane normal in the intermediates K, L, and M in the photocycle of bR. We found very clear and reproducible differences in the anisotropies of the various intermediates (see Figures 10b and 11b) which translate however into only small changes in the angle ($\Delta\theta \leq 2°$). This illustrates the high sensitivity of our method. Isotropic excitation on oriented samples allows nearly saturating excitation intensity, resulting in an excellent signal to noise ratio. In contrast, photoselection experiments require infinitesimal excitation, with a correspondingly low signal to noise ratio. Photoselection experiments have been performed either on isotropic samples[6,8,26] (suspension or PM immobilized in a gel) or on oriented samples.[10,11] Measurements in isotropic systems only provide information about changes in the orientation of the transition dipole moment with respect to the bR ground state ($\Delta\Omega_i$), while the use of oriented samples supplies information on both the change in polar ($\Delta\theta_i$) and azimuthal ($\Delta\phi_i$) angle of the transition dipole moment in the membrane frame. In both cases, contradictory results have been reported. The authors of ref 26 obtained $\Delta\Omega_K = 11°$, $\Delta\Omega_L = 17°$, and $\Delta\Omega_M = 20°$; in ref 6 it was found that $\Delta\Omega_K \leq 10°$, whereas in ref 8 a constant anisotropy was reported from 50 ns to 50 μs, which implies that the transition dipole moment rotates by less than 8° (experimental sensitivity) in this time domain. According to ref 26, immobilization of the purple membranes in a polyacrylamide gel reduces chromophore reorientations in L and M but does not eliminate them. The reader should remember, however, that the sensitivity of these experiments is low. Moreover, there is no evidence that the photochemical, functional, and spectral properties of purple membranes might be affected by the gel (photocycle, light−dark adaptation). The authors of ref 26 previously postulated the so-called spectator model,[7] where they assumed that the chromophores of the nonphotocycling bR molecules in the trimer reorient during the photocycle. This response was attributed to cooperativity in the trimer, but it is not known what kind of interaction between the monomers might be involved. The previous measurements on oriented purple membrane samples[9,10] showed that the transition dipole moment tilts out of the membrane plane by about 3° in the M intermediate. In contrast, in a recent publication,[11] a considerably larger reorientation of 14° was reported in the same direction during the M state. In the intermediates K and L, these authors observed reorientation of only 3° also in the same direction. No in-plane reorientations larger than the uncertainties (±7°) were detected.[11]

Using isotropic excitation, information about in-plane reorientation (changes of the azimuthal angle of the transition dipole moment in the membrane frame) is lost for symmetry reasons. Since strong and even saturating excitation is applied, the signals are less noisy and the theoretical expressions become quite simple. Thus the information about out-of-plane reorientation is much more accurate than in the photoselection experiments. With respect to the orientation of the bR ground state, we found for wildtype $\Delta\theta_K = -0.7 \pm 0.3°$, $\Delta\theta_L = -1.7° \pm 0.3°$, and $\Delta\theta_M = -0.8 \pm 0.5°$. The latter value is slightly smaller but qualitatively in good agreement with our previous measurements.[10] More reliable results for M and L were obtained with the mutant D96A. The angular changes for the four sets of experiments are summarized in Table 1. We note that in spite of the very different time courses of the intermediates in these experiments, the anisotropies are essentially the same. Taking the average over all the results of Table 1, we find $\Delta\theta_K = -0.8 \pm 0.2°$, $\Delta\theta_L = -1.7 \pm 0.2°$, and $\Delta\theta_M = -1.1 \pm 0.3°$. We have no explanation for the discrepancy of our results with those of ref 11, in particular for M. Since we measured in our experiments the linear birefringence change as an independent parameter, we have an additional control (using the Kramers−Kronig transform) that the transient linear dichroism data were correctly determined. Moreover, there was no need in our data analysis to introduce the ad hoc assumption of spectator chromophores, and we considered the orientation of the transition dipole moment of the nonexcited molecules as unaffected during the photocycle of the excited molecules.

For the mutant D96A at pH 7, 20 °C, the time trace of the anisotropy at 410 nm remained constant from 100 μs to 1 s. This confirms earlier observations with wild type.[9] There is thus no evidence from our data for the existence of two M states with different anisotropies and chromophore orientations in this time domain. Multiple M states may have been expected in the framework of a reprotonation switch model in which the Schiff base accessibility changes during the M lifetime from D85 to D96.

The small changes in the transition dipole moment in the intermediates K, L, and M suggest a model of reorientation of the retinal, which was already discussed in detail in ref 10. The 13-cis isomerization is associated with a motion of the C_{20} methyl group toward the cytoplasmic side of the membrane, while the C_5-N direction reorients only slightly (<2°). A tilt of the C_5-C_{13} part of the polyene chain out of the membrane plane is also supported by ^2H NMR studies which indicate that the angle between the $C_{19}-C^2H_3$ bond and the membrane normal increases by 7° in the M intermediate.[28] In-plane neutron diffraction studies[27] showed, moreover, that the cyclohexene ring position does not change between the groundstate and the M state. Since it is unlikely that the length of the polyene chain increases, the N atom of the Schiff base has to move toward the ring. This would require a certain flexibility of the Lys-216 side chain.

In this paper, we showed that using a few plausible physical constraints, the spectra, anisotropies, and time courses of the early intermediates of bacteriorhodopsin could be obtained in a unique way from the transient absorbance changes provided the transient linear dichroism data were included in the analysis. Similar problems with spectrally and kinetically overlapping intermediates occur with other photobiological systems and the methods presented here may find more general application. For a number of photoreceptors such as rhodopsin, sensory rhodopsin, phytochrome, and the photoactive yellow protein transient chromophore reorientations are expected to occur. Provided these proteins can be oriented, the methods developed here to determine the change in transition dipole moment orientation may be applied to those systems too.

Acknowledgment. We are greatly indebted to Stefan Dickopf for experimental support and helpful suggestions. We thank Martin Kanowski, Werner Hoffmann, and Klaus Lüders (Freie Universität Berlin) for allowing us to use their 14 T magnet. This research was supported by the Deutsche Forschungsgemeinschaft, grant He1382/7-2 and the Ständige Kommission für Forschung und Wissenschaftlichen Nachwuchs (FNK), Freie Universität Berlin, 02/524 01.

References and Notes

(1) Mathies, R. A.; Lin, S. W.; Ames, J. B.; Pollard, W. T. *Annu. Rev. Biophys. Biophys. Chem.* **1991**, *20*, 491−518.

(2) Jäger, S.; Lewis, J. W.; Zvyaga, T.; Szundi, I.; Sakmar, T. P.; Kliger, D. S. *Proc. Natl. Acad. Sci. U.S.A.* **1997**, *94*, 8557−8562.

(3) Kendrick, R. E.; Kronenberg, G. H. M., Eds. *Photomorphogenesis in Plants*, 2nd ed.; Kluwer Academic: Dordrecht, The Netherlands, 1994.

(4) Meyer, T. E.; Yakali, E.; Cusanovich, M. A.; Tollin, G. *Biochemistry* **1987**, *26*, 418−423.

(5) Genick, U. K.; Soltis, S. M.; Kuhn, P.; Canestrelli, I. L.; Getzoff, E. D. *Nature* **1998**, *392*, 206−209.

(6) Karvaly, B.; Fukumoto, J. M.; Hopewell, W. D.; El-Sayed, M. A. *J. Phys. Chem.* **1982**, *86*, 1899−1908.

(7) Wan, C.; Qian, J.; Johnson, C. K. *Biophys. J.* **1993**, *65*, 927−938.

(8) Esquerra, R. M.; Che, D.; Shapiro, D. B.; Lewis, J. W.; Bogomolni, R. A.; Fukushima, J.; Kliger, D. S. *Biophys. J.* **1996**, *70*, 962−970.

(9) Otto, H.; Heyn, M. P. *FEBS Lett.* **1991**, *293*, 111−114.

(10) Heyn, M. P.; Otto, H. *Photochem. Photobiol.* **1992**, *56*, 1105−1112.

(11) Song, Q.; Harms, G. S.; Johnson, C. K. *J. Phys. Chem.* **1996**, *100*, 15605−15613.

(12) Otto, H.; Zscherp, C.; Borucki, B.; Heyn, M. P. *J. Phys. Chem.* **1995**, *99*, 3847−3853.

(13) Zimányi, L.; Lanyi, J. K. *Biophys. J.* **1993**, *64*, 240−251.

(14) Nagle, J. F.; Zimányi, L.; Lanyi, J. K. *Biophys. J.* **1995**, *68*, 1490−1499.

(15) Gergely, C.; Zimányi, L.; Váró, G. *J. Phys. Chem.* **1997**, *101*, 9390−9395.

(16) Nagle, J. F. *Biophys. J.* **1991**, *59*, 476−487.

(17) Borucki, B.; Otto, H.; Heyn, M. P. *J. Phys. Chem. B* **1998**, *102*, 3821−3829.

(18) Govindjee, R.; Balashov, S. P.; Ebrey, T. G. *Biophys. J.* **1990**, *58*, 597−608.

(19) Hofrichter, J.; Henry, E. R.; Lozier, R. H. *Biophys. J.* **1989**, *56*, 693−706.

(20) Heyn, M. P.; Cherry, R. J.; Müller, U. *J. Mol. Biol.* **1977**, *117*, 607−620

(21) Lin, S. W.; Mathies, R. A. *Biophys. J.* **1989**, *56*, 653−660

(22) Otto, H.; Marti, T.; Holz, M.; Mogi, T.; Lindau, M.; Khorana, H. G.; Heyn, M. P. *Proc. Natl. Acad. Sci. U.S.A.* **1989**, *86*, 9228−9232.

(23) Tkachenko, N. V.; Savransky, V. V.; Sharonov, A. Y *Eur. Biophys. J.* **1989**, *17*, 131−136.

(24) Zeisel, D.; Hampp, N. *J. Phys. Chem.* **1992**, *96*, 7788−7792.

(25) Lewis, J. W.; Kliger, D. S. *Photochem. Photobiol.* **1991**, *54*, 963−968.

(26) Song, Q.; Harms, G. S.; Wan, C.; Johnson, C. K. *Biochemistry* **1994**, *33*, 14026−14033.

(27) Hauss, T.; Büldt, G.; Heyn, M. P.; Dencher, N. A. *Proc. Natl. Acad. Sci. U.S.A.* **1994**, *91*, 11854−11858.

(28) Moltke, S.; Wallat, I.; Sakai, N.; Nakanishi, K.; Brown, M. F.; Heyn, M. P. *Biochemistry*, in press.